25.4: Active Structural Error Suppression in MEMS Vibratory Gyroscopes

Chris C. Painter
Mechanical and Aerospace Engineering
University of California, Irvine
Irvine, CA, USA
cpainter@uci.edu

Andrei M. Shkel
Mechanical and Aerospace Engineering
University of California, Irvine
Irvine, CA, USA
ashkel@uci.edu

Abstract

Due to restrictive tolerancing, structural imperfections that reduce performance of fabricated micro devices are typical. While feedback control is normally used to compensate for these imperfections, we show that this is insufficient for suppressing errors without interfering with device performance. The only alternatives are costly and time consuming post processing or the implementation of a dual stage control architecture comprised of a feedforward and feedback control which compensates for errors without interfering with the performance of the device. In this paper, we describe the design and implementation of such a control architecture for structural error suppression in MEMS vibratory gyroscopes. The feedforward portion of the control is used to "trim" large imperfections, while the feedback portion compensates for the remaining non-idealities and perturbations. The architecture includes self-diagnostic capabilities for in situ identification of structural imperfections used to set the feedforward control forces. The realization of this dual stage control architecture is demonstrated in a device using non-linear electrostatic parallel plate actuators. We demonstrate successful compensation for a device with 10% error in ideal stiffness subjected to a further 1% perturbation during normal operation.

Keywords

MEMS, Rate Integrating Gyroscopes, Smart MEMS, Electrostatic Trimming

INTRODUCTION

In its current maturity, fabrication technologies fall below the tolerancing required for high precision devices, requiring active feedback control or post processing such as laser trimming or selective material deposition[1] to achieve design goals. This demand gives rise to devices with enhanced capabilities, such as structural compensation, self-calibration, and signal processing integrated on the same chip. To operate with the highest precision, vibratory gyroscopes [2, 3] typically include on-chip feedback control to compensate for fabrication imperfections. However, as will be illustrated in this paper, when imperfections are large compared to the measured Coriolis force, compensation cannot be achieved with a purely feedback control without interfering with the Coriolis measurements. Preliminary study of a prototype rate integrating gyroscope illustrates an example of a device with large structural imperfections where a purely feedback control could not be used [4].

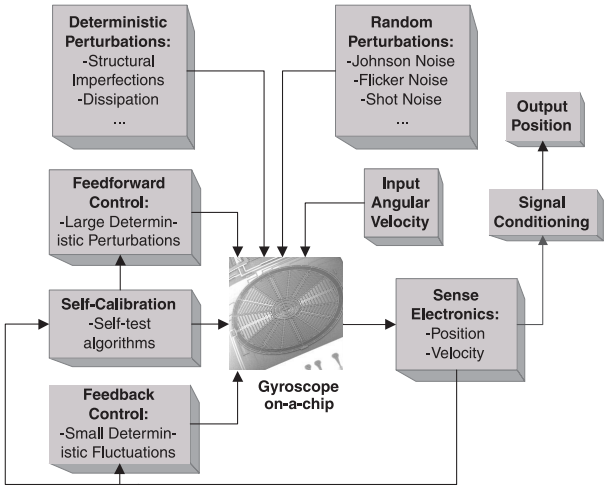

Figure 1. A "smart" MEMS gyroscope would include self-calibration capabilities built on-chip for detection and compensation of deterministic perturbations.

The only alternative to using a purely feedback control system that avoids the necessity for costly post processing is the implementation of a dual stage architecture that utilizes both feedforward and feedback control (Figure 1). A gyroscope using this architecture would be fabricated with self-calibration capabilities that enable the device to identify its own system characteristics such as stiffness and damping utilizing an on-chip self-test algorithm. With these self-calibrative capabilities, the device can identify structural imperfections and compensate for them with the feedforward portion of the control architecture (i.e., electrostatic "trimming"). The feedforward control would work in unison with the feedback control that compensates for small perturbations arising during the normal operation of the device.

GYROSCOPE DYNAMICS

The studied MEMS gyroscope [5] consists of a distributed mass with stationary parallel plate electrodes interwoven throughout the mass for electrostatic drive and sense

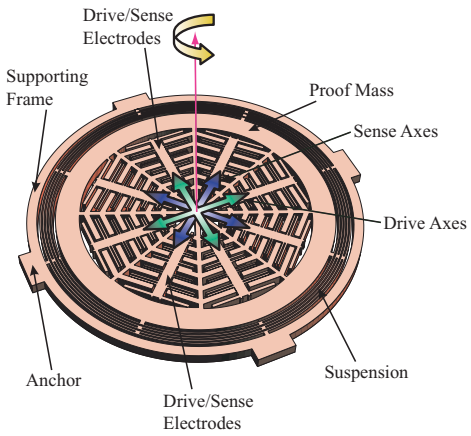

Figure 2. The studied rate integrating gyroscope [5] consists of a freely vibrating proof mass attached to a concentric six ring suspension. Stationary electrodes interwoven throughout the mass sustain motion and allow measurement of the Coriolis induced precession angle. The precession angle is proportional to the angle of rotation of the device.

(Figure 2). The mass is suspended on a six interconnected ring suspension which provides necessary stiffness isotropy required for the successful operation of the device [4]. The device has been modeled as a lumped mass-spring system operating in its first two fundamental in-plane modes (Figure 3a). The lumped mass-spring dynamics of an ideal system are expressed in the rotating coordinate frame (x,y) by [6]

$$\begin{aligned} \ddot{x} + \omega_n^2 x - 2\Omega\dot{y} &= 0 \\ \ddot{y} + \omega_n^2 y + 2\Omega\dot{x} &= 0 \end{aligned} \tag{1}$$

where ω_n is the natural frequency and Ω is the input angular velocity. If the system is initially freely vibrating, over time the line of oscillation will precess by an angle ϕ with respect to the moving coordinate frame (Figure 3b and Figure 7a). The precession angle, which can be instantly identified as

$$\tan\phi = \frac{2\left(\omega_n^2 xy + \dot{x}\dot{y}\right)}{\omega_n^2\left(x^2 - y^2\right) + \left(\dot{x}^2 - \dot{y}^2\right)} \tag{2}$$

is proportional to the angle of rotation of the moving frame. Anisoelasticities due to fabrication imperfections disrupt isotropy of the suspension, causing frequency mismatch and mode coupling. Assuming negligible non-linear effects, the equations of motion with these stiffness non-idealities become

$$\begin{aligned} m\ddot{x} + k_{xx}x + k_{xy}y - 2m\Omega\dot{y} &= 0 \\ m\ddot{y} + k_{yy}y + k_{yx}x + 2m\Omega\dot{x} &= 0 \end{aligned} \tag{3}$$

where m is the lumped mass approximation for the gyroscope and k_{xx}, k_{yy}, k_{xy}, and k_{yx} are the non-ideal stiffness terms. The non-ideal stiffness terms can be interpreted as perturbations from an ideal isotropic stiffness k_n. In terms of the principal stiffness values K_1 and K_2 and the angular mismatch angle α of the principal axes of elasticity with the x-y coordinate system (Figure 4), the stiffness non-idealities are written as [7]

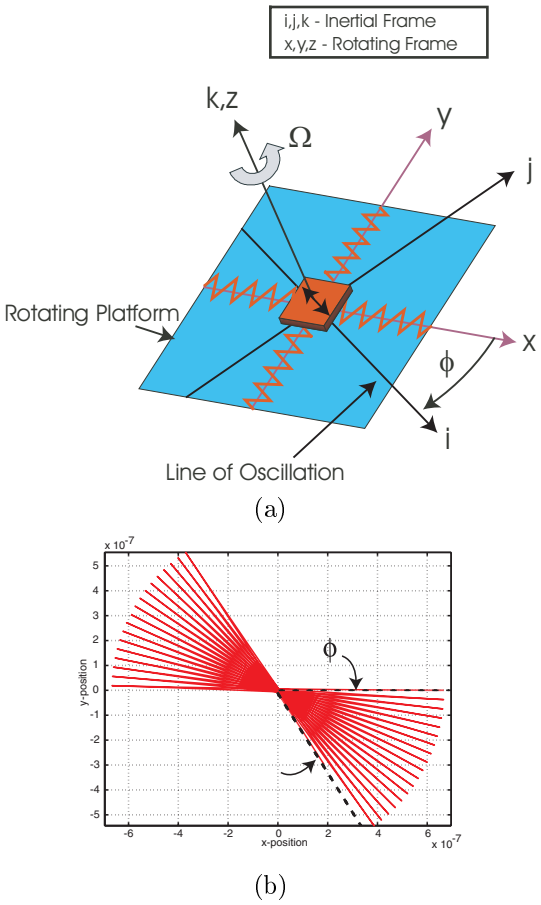

Figure 3. (a) The gyroscope is modeled as a two degree of freedom lumped mass-spring system. $\{i, j, k\}$ is the inertial coordinate system and $\{x, y, z\}$ is the coordinate system attached to the rotating platform. (b) In the presence of an input angular rotation, the line of oscillation would be observed to precess by an angle ϕ with respect to the rotating coordinate system.

$$\begin{aligned} k_{xx} &= k_n + h\cos(2\alpha) \\ k_{yy} &= k_n - h\cos(2\alpha) \\ k_{xy} &= k_{yx} = h\sin(2\alpha) \end{aligned} \tag{4}$$

where $2k_n = (K_1 + K_2)$ and h is proportional to the stiffness mismatch between the principal axes, $2h = (K_1 - K_2)$. An appropriate feedback control which will compensate for anisoelasticity while not interfering with the Coriolis force is of the form [6]

$$\begin{Bmatrix} F_x \\ F_y \end{Bmatrix} = -\gamma_1 \cdot P \cdot S^T \cdot \begin{Bmatrix} x \\ y \end{Bmatrix} \tag{5}$$

where γ_1 is a constant gain, S is a 2×2 skew symmetric matrix, and P is quadrature defined as

$$P = \pi\left(x\dot{y} - y\dot{x}\right) \tag{6}$$

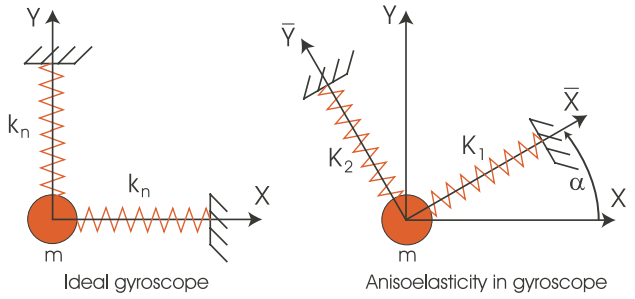

Figure 4. In the ideal gyroscope, the principal axes of elasticity have equal stiffness (k_n) and coincide with the x-y coordinate system. In the presence of imperfections, there is a mismatch in the principal stiffness values, $2h = (K_1 - K_2)$ and an angular mismatch of the principal axes from the x-y coordinate system by an angle α.

It is guaranteed that the feedback controller will compensate for imperfections while not interfering with the Coriolis force as long as the imperfections are sufficiently small (e.g., $\alpha = 10$ degrees and h corresponds to 1% of the ideal stiffness, Figure 7f,g). For larger errors (e.g., $\alpha = 10$ degrees and h corresponds to 10% of the ideal stiffness) the controller, while compensating for the errors, also interferes with the measured precession angle (Figure 7b,c). One fabricated prototype gyroscope (Figure 5) shows much larger errors ($\alpha = 45$ and h corresponds to 72% of the ideal stiffness) and while this is an extreme example and can vary from run to run and device to device, it illustrates that some level of structural imperfections will always be present. Thus, it is necessary to implement a feedforward control to compensate for the imperfections, which is guaranteed not to interfere with measured precession angle (Figure 7e), while retaining a feedback control to correct for small uncompensated errors developing during normal operation of the device.

IDENTIFICATION OF ERRORS

The basis for developing the feedforward portion of the control is the identification of structural imperfections. From the dynamic response of the device, an on-chip self-test algorithm [8] is implemented that extracts the structural non-idealities of the system. Based off the interpretation of anisoelasticity given in (4), the algorithm uses principal component analysis (PCA) to first identify the angle of misalignment α. Parameters k_n and h are then identified through the sum and difference, respectively, of the eigenfrequencies in the principal coordinate system using a Fourier transform of the dynamic system response. The feedforward control is implemented using forces proportional to the anisoelasticity parameters h and α. The realization of this control using non-linear electrostatic actuators is described next.

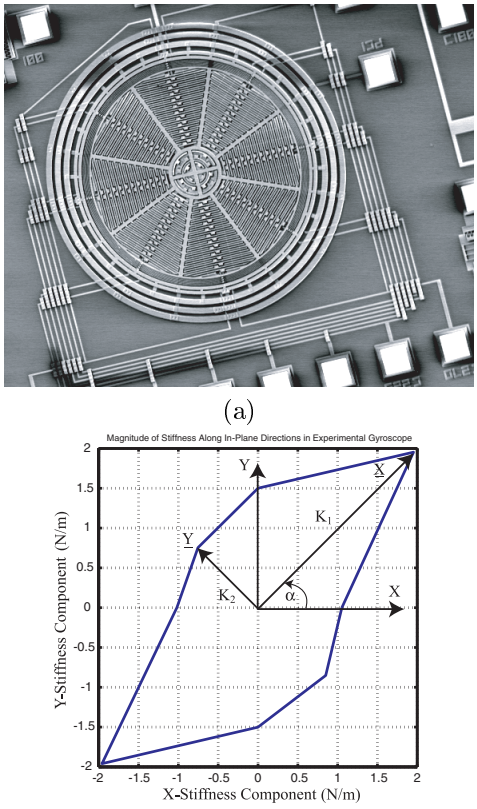

Figure 5. (a) A prototype surface machined rate integrating gyroscope was fabricated using JDS Uniphase's MUMPS process. (b) In the prototype gyroscope, the stiffness along the four axes is estimated by observing the natural frequency along each direction and knowing the ideal mass of the system. The plot of stiffness magnitude along the four directions shows large mismatches between the principal axis stiffnesses K_1 and K_2 ($\frac{K_1-K_2}{K_1+K_2} = 72\%$) and coupling (rotation of the stiffness axes by angle $\alpha = 45$).

DUAL STAGE ELECTROSTATIC CONTROL

Electrostatic "Trimming"

Two different physical mechanisms were reported in MEMS for active frequency tuning, thermal compensation [9] and electrostatic tuning [2]. Since the angular gyroscope utilizes parallel plate electrodes for drive and sense, we focus on using the inherent non-linearity of the electrostatic forces to tune out the non-ideal components of the stiffness matrix (Figure 6). The non-ideal dynamics of the gyroscope, including the electrostatics, can be expressed by

$$m\ddot{x} + (k_n + h\cos 2\alpha)\, x + (h \sin 2\alpha)\, y = F_{e,x} \quad (7)$$

$$m\ddot{y} + (h \sin 2\alpha)\, x + (k_n - h\cos 2\alpha)\, y = F_{e,y} \quad (8)$$

where $F_{e,x}$ and $F_{e,y}$ are electrostatic forces expressed as

$$\frac{2F_{e,i}}{\epsilon_0 t} = \frac{g - Nj}{(d-i)^2} V_{i,1}^2 + \frac{g + Nj}{(d-i)^2} V_{i,2}^2 -$$

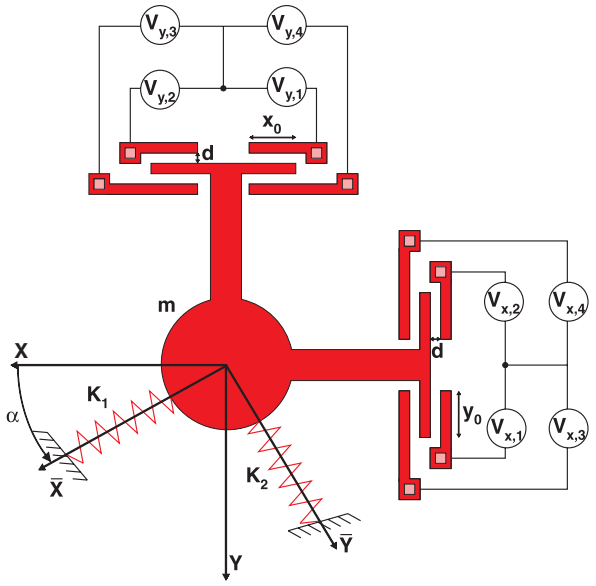

Figure 6. We use the inherent non-linearity of the parallel plate actuators along the x and y directions in order to tune out the non-ideal stiffness elements.

$$\frac{g-Nj}{(d+i)^2}V_{i,3}^2 - \frac{g+Nj}{(d+i)^2}V_{i,4}^2 + \frac{N}{d-j}V_{j,1}^2 - \frac{N}{d-j}V_{j,2}^2 - \frac{N}{d+j}V_{j,3}^2 + \frac{N}{d+j}V_{j,4}^2$$

Here $\{i,j\} = \{x,y\}$ and $\{y,x\}$, N is the number of control electrode sets (e.g., in Figure 6, N = 1), t is the structural thickness, d is the parallel plate gap, g is the total plate overlap ($g = Nx_0 = Ny_0$), and ϵ_0 is the permittivity of a vacuum. For structural compensation, we use the following control voltages [2]

$$\begin{array}{ll} V_{x,1} = V_{DC} + v_{xq} + v_x & V_{x,2} = V_{DC} - v_{xq} + v_x \\ V_{x,3} = V_{DC} - v_{xq} - v_x & V_{x,4} = V_{DC} + v_{xq} - v_x \\ V_{y,1} = V_{DC} - v_{yq} + v_y & V_{y,2} = V_{DC} + v_{yq} + v_y \\ V_{y,3} = V_{DC} - v_{yq} - v_y & V_{y,4} = V_{DC} + v_{yq} - v_y \end{array} \quad (9)$$

where V_{DC} is a constant bias voltage, v_{xq} and v_{yq} are constant feedforward quadrature control voltages and v_x and v_y are state dependent feedback control voltages. We determine the voltages for the feedforward quadrature control by first assuming zero feedback ($v_x = v_y = 0$). The non-linearity of the parallel plates leads to a non-zero first derivative of the electrostatic force with respect to position, which can be interpreted as an electrostatic spring [2], contributing to the overall system stiffness. In order to find a closed-form approximation for the control voltages, we assume small deflections and combine the ideal (K_i), non-ideal (K_n), and electrostatic (K_e) matrix contributions together to form the overall stiffness realization

$$\begin{aligned} K &= K_i + K_n + K_e \quad (10)\\ K_i &= \begin{bmatrix} k_n & 0 \\ 0 & k_n \end{bmatrix} \\ K_n &= \begin{bmatrix} h\cos(2\alpha) & h\sin(2\alpha) \\ h\sin(2\alpha) & -h\cos(2\alpha) \end{bmatrix} \\ K_e &= \frac{4\epsilon_0 t}{d^2}\begin{bmatrix} \Phi_1 & \Phi_2 \\ \Phi_2 & \Phi_3 \end{bmatrix} \\ \Phi_1 &= -\frac{g}{d}\left(V_{DC}^2 + v_{xq}^2\right) \\ \Phi_2 &= \left(V_{DC}v_{xq} + V_{DC}v_{yq}\right) \\ \Phi_3 &= -\frac{g}{d}\left(V_{DC}^2 + v_{yq}^2\right) \end{aligned}$$

With any arbitrary DC voltage, there exists an appropriate set of control voltages v_{xq} and v_{yq} to cancel the off-diagonal terms of the stiffness matrix and set the on-diagonal stiffness terms equal to each other (k_{tuned}).

$$v_{xq} = \frac{-d\left(8\cos(2\alpha)\epsilon_0 t N^2 V_{DC}^2 + gh\sin^2(2\alpha)d\right)}{8g\sin(2\alpha)N\epsilon_0 t V_{DC}} \quad (11)$$

$$v_{yq} = \frac{-d\left(-8\cos(2\alpha)\epsilon_0 t N^2 V_{DC}^2 + gh\sin^2(2\alpha)d\right)}{8g\sin(2\alpha)N\epsilon_0 t V_{DC}} \quad (12)$$

Parameters h and α represent the principal axes stiffness mismatch and angle of misalignment between the coordinate axes and the principal axes of elasticity, respectively, that have been determined using a self-test algorithm [8]. Because the on-diagonal electrostatic stiffness term is always negative, the tuned on-diagonal stiffness values will always be less than the original ideal stiffness ($k_{tuned} < k_n$). To take this into account, a good strategy is to design the gyroscope suspension to be stiffer than desired. A fundamental limit is reached when these stiffness terms become negative ($k_{tuned} < 0$) and the system becomes unstable. Thus, an optimal DC bias voltage is one that maximizes the trace of the stiffness matrix subject to the constraint that v_{xq} and v_{yq} must satisfy (11) and (12). This optimal DC voltage is found to be

$$V_{DC}^2 = sign\{h\} \cdot \frac{hg\left(1-\cos(2\alpha)^2\right)d^2}{8\epsilon_0 N\sqrt{(d^2N^2-g^2)\cos(2\alpha)^2 + g^2}} \quad (13)$$

Since v_{xq} and v_{yq} are functions of the bias voltage, the choice of sign of V_{DC} is arbitrary. Even with an optimal choice for bias voltage, invariably a limit is reached where system instability is inevitable. This limit in terms of anisoelasticity parameters h and α is

$$\left|\frac{h}{k_n}\right| < \frac{dN}{\sqrt{(d^2N^2-g^2)\cos(2\alpha)^2 + g^2}} \quad (14)$$

In the given device (Figure 2), there are four different sets of axes that can, in principle, be used as the

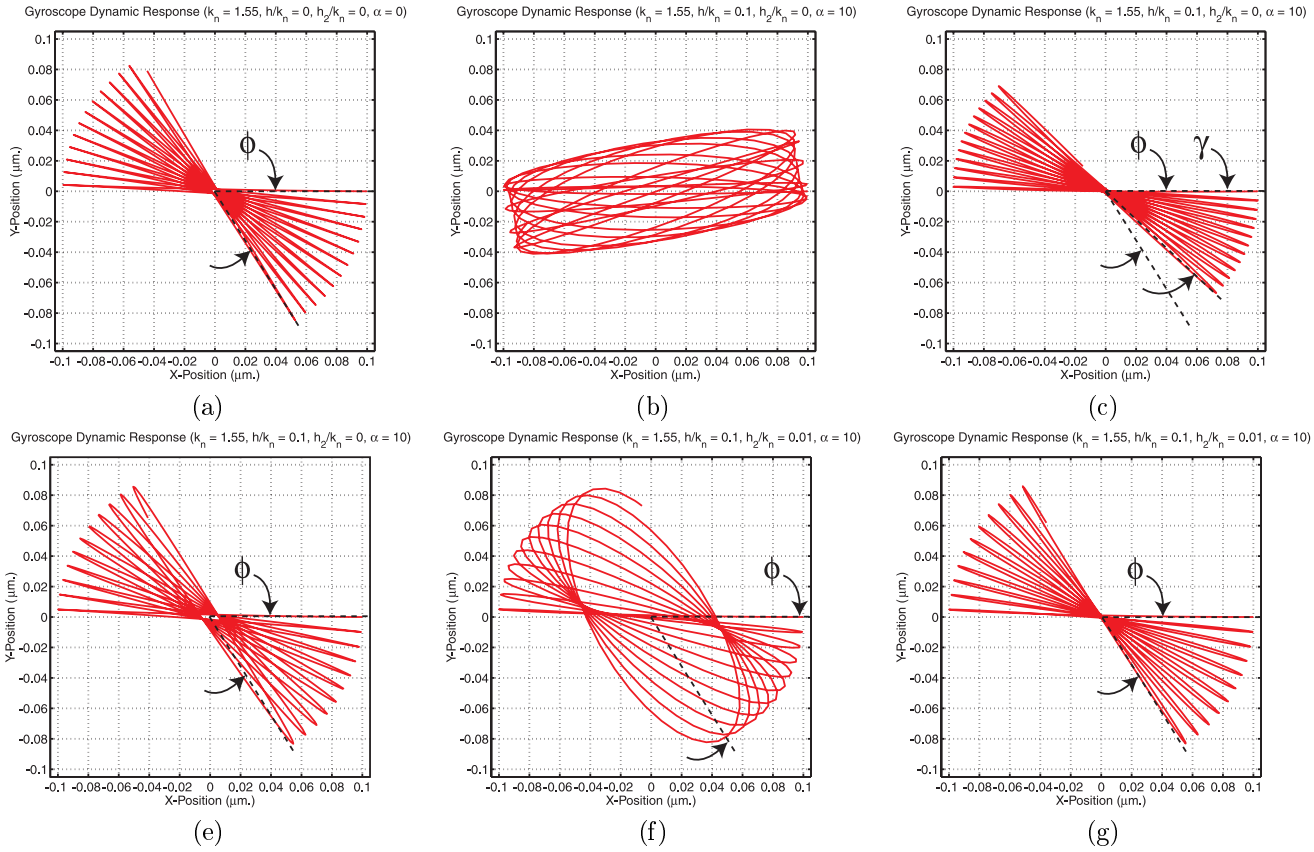

Figure 7. (a) In the absence of imperfections, the line of oscillation precesses normally by angle ϕ in the presence of an input angular rotation. (b) Large anisoelasticities due to fabrication imperfections interfere with the ideal operation of the device, eliminating the precession. (c) The feedback control used to compensate for these large imperfections also interferes with the precession pattern, reducing the precession angle from the ideal angle ϕ to γ. (d) By using a feedforward control, large structural anisoelasticities can be eliminated while maintaining the ideal precession of the device. (e) While the feedforward control can compensate for constant structural imperfections, it is invariant to small perturbation that arise during normal operation of the device (e.g., due to thermal fluctuations), which disrupt the line of oscillation. (f) A dual-stage feedforward/feedback architecture can compensate for both structural imperfections and small perturbations without interfering with the precession.

operational drive axes. Thus, the largest angle of misalignment is $\alpha < \frac{\pi}{8}$ and in this limit, (14) reduces to

$$\left|\frac{h}{k_n}\right| < \frac{2dN}{\sqrt{2d^2N^2 + 2g^2}} \tag{15}$$

Feedback Control

While the feedforward control can compensate for large constant structural imperfections, it is also necessary to implement a feedback control to correct for small fluctuations that arise during the normal operation of the device. For the feedback control, we implement state dependent control voltages v_x and v_y

$$v_x = \frac{d^2\left(Ndv_{yq}F_y + F_x g V_{DC}\right)}{4\epsilon_0 t\left(g^2V_{DC}^2 - N^2d^2v_{xq}v_{yq}\right)} \tag{16}$$

$$v_y = \frac{d^2\left(Ndv_{xq}F_x + F_y g V_{DC}\right)}{4\epsilon_0 t\left(g^2V_{DC}^2 - N^2d^2v_{xq}v_{yq}\right)} \tag{17}$$

where F_x and F_y are the control forces based off the skew symmetric control architecture given in (5). This architecture is guaranteed of compensating for small perturbations without interfering with the Coriolis induced precession. With the addition of the feedforward control voltages, the complete dual stage architecture is capable of "trimming" large structural imperfections while compensating for small perturbations. Computer simulations are presented to demonstrate the effectiveness of this system.

Numerical Simulation

All simulation parameters are based off a realistic implementation of a surface micromachined rate integrating gyroscope (Figure 5). The mass of the device is 4.10×10^{-10}kg and the isotropic stiffness k_n is 1.55 N/m, giving a natural frequency of 9.8 kHz for the system. The total parallel plate overlap g is 1200 μm, the parallel plate gap d is 2 microns, and the permittivity ϵ_0 is 8.854×10^{-12} F/m. The simulations are based off

the non-linear equations of motion (7), using an initial x deflection of .1 microns to satisfy the small deflection assumption. For a chosen set of large structural anisoelasticities ($h/k_n = 10\%, \alpha = 10$ deg.), the optimal DC bias voltage is calculated from (13) to be 5.35 V, which will remain constant for each simulation. Under this bias voltage and in the absence of imperfections (h = 0, $\alpha = 0$), the line of oscillation precesses by an angle ϕ (Figure 7a). With large structural anisoelasticities ($h/k_n = 10\%, \alpha = 10$ deg.) and without compensation ($v_{xq} = v_{yq} = v_x = v_y = 0$), the system oscillates about the principal axes of elasticity and there is no precession (Figure 7b). A purely feedback control using control voltages v_x and v_y as calculated from (16) and (17) is then attempted, which eliminates the quadrature error, but also interferes with the precession angle (Figure 7c). Next, based off algorithms used in [8], the calculated non-ideal stiffness parameters h and α are found as would be determined by the on-chip self-test ($(h/k_n)_{calc} = 10.23\%, \alpha_{calc} = 10.16$ deg.). These calculated h and α parameters are used to find the appropriate compensating feedforward control voltages v_{xq} and v_{yq} as given by (11) and (12). The purely feedforward control ($v_x = v_y = 0$), is used to eliminate the quadrature error, which allows ideal precession of the line of oscillation (Figure 7d). To realize the effect of additional small perturbations, we add small anisoelasticities ($h_2/k_n = 1\%$) to the system that are not compensated for by the feedforward control (e.g., due to thermal fluctuations), which result in destruction of the precession pattern (Figure 7e). A dual-stage control architecture consisting of the feedforward control plus the feedback control, is used to compensate for both large structural imperfections and small perturbations while still allowing the undisturbed precession of the line of oscillation (Figure 7f).

CONCLUSION

In this paper, we have demonstrated the necessity for a dual stage control architecture comprising feedforward and feedback control systems in order to compensate for fabrication imperfections prevalent in micromachined gyroscopes. We have shown how this control can be realized in a gyroscope using electrostatic parallel plates. The successful application of feedforward control was shown in a device with large structural imperfections of 10% of the ideal stiffness where a purely feedback control would interfere with the performance of the device. Additionally, the feedback portion of the control was shown to compensate for a further 1% error to the stiffness as a result of small perturbations arising during normal operation. We have given an expression for the fundamental error suppression limit of the electrostatic implementation of this dual stage architecture. In the case of devices with imperfections beyond this limit, it is necessary to employ alternative methods such as thermal tuning or post processing. Future work includes study of additional capabilities for identification and suppression of damping, experimental demonstration of the dual stage architecture using a DSP implementation, and implementation using on-chip CMOS control circuitry.

ACKNOWLEDGEMENTS

The author would like to thank the Department of Defense who is sponsoring this work through a 2001 National Defense Science and Engineering Graduate Fellowship.

REFERENCES

[1] D. Joachim and L. Lin, "Selective polysilicon deposition for frequency tuning of MEMS resonators," in IEEE MEMS 2002, Las Vegas, NV, January 2002.

[2] W. A. Clark, Micromachined Vibratory Rate Gyroscopes. PhD thesis, UC Berkeley, 1997.

[3] M. Putty, and K. Najafi, "A micromachined vibrating ring gyroscope," in IEEE Solid State Sensors and Actuators Workshop, pp. 213–220, Hilton Head Island, SC, June 1996.

[4] C. Painter and A. Shkel, "Structural and thermal modeling of a MEMS angular gyroscope," in 2001 SPIE Annual International Symposium on Smart Structures and Materials, Newport Beach, CA, March 2001.

[5] A. Shkel and R. T. Howe, "Polysilicon Surface Micromachined Rate Integrating Gyroscopes." UC-Berkeley Office of Technology and Licensing. Case Number B99-077.

[6] A. Shkel, R. Horowitz, A. Seshia, and R.T. Howe, "Dynamics and control of micromachined gyroscopes," in The American Control Conference, pp. 2119–2124, San Diego, CA, June 1999.

[7] A. Shkel, R.T. Howe, and R. Horowitz, "Modeling and simulation of micromachined gyroscopes in the presence of imperfections," in 1999 International Conference on Modeling and Simulation of Microsystems, pp. 605–608, San Juan, Puerto Rico, April 1999.

[8] C. Painter and A. Shkel, "Identification of anisoelasticity for electrostatic "trimming" of rate integrating gyroscopes," in 2002 SPIE Annual International Symposium on Smart Structures and Materials, San Diego, CA, March 2002.

[9] T. Remtema and L. Lin, "Active Frequency Tuning for Microresonators by Localized Thermal Stressing Effects," in Solid-State Sensor and Actuator Workshop, pp. 363–366, Hilton Head Island, SC, June 2000.